

Multiscale Sparsifying Transform Learning for Image Denoising

Ashkan Abbasi^a, Amirhassan Monadjemi^{b,*}, Leyuan Fang^{c,*}, Hossein Rabbani^d, Neda Noormohammadi^a, and Yi Zhang^e

^a Artificial Intelligence Department, Faculty of Computer Engineering, University of Isfahan, Isfahan, Iran.

^b School of Continuing and Lifelong Education, National University of Singapore, Lower Kent Ridge Road, Singapore. (E-mail: sleam@nus.edu.sg)

^c College of Electrical and Information Engineering, Hunan University, Changsha, China. (E-mail: fangleyuan@gmail.com)

^d Department of Biomedical Engineering, Medical Image and Signal Processing Research Center, School of Advanced Technologies in Medicine, Isfahan University of Medical Sciences, Isfahan, Iran.

^e College of Computer Science, Sichuan University, Chengdu, China.

* indicates the corresponding author.

Abstract—The data-driven sparse methods such as synthesis dictionary learning (e.g., K-SVD) and sparsifying transform learning denoising (TLD) have been proven effective in image denoising. However, they are intrinsically single-scale which can lead to suboptimal results. In this paper, we firstly employ the strategy of denoising wavelet subbands, and show its shortcomings. Then, we show that this strategy can be enhanced using wavelet subbands mixing to combine the merits of both the single and multiscale methods. In contrast to Fused K-SVD, which is a method that takes tens of seconds to fuse the results of the single and multiscale methods through a joint sparse model over a learnt dictionary, our proposed fusion method takes less than one second, has comparable performance, and does not depend on pre-training. Finally, we show that we can devise an efficient multiscale method without the need for denoising detail subbands. This method proposes a systematic way of using the pyramid of low-pass subbands of discrete wavelet transform for image denoising. We analyze and assess the studied methods through the experiments over different datasets. The experiments show that our methods offer good trade-offs between performance and complexity, and also perform favorably well in removing real noise from fluorescence microscopy images in comparison with some representative multiscale methods.

Index Terms— Sparsifying Transform Learning, Multiscale Sparse Representations, Wavelets, Natural Image Denoising, Fluorescence Microscopy Denoising (FMD).

1 INTRODUCTION

Sparse models have been proven effective in various image restoration and compression problems. One approach to exploit the notion of sparsity is based on fixed transform models (such as discrete cosine transform (DCT) [1] and wavelets [2]). In these models, the analysis and synthesis filters are derived based on a mathematical model of the data and desired characteristics, leading to highly structured transforms with fast implementations. In addition to their computational efficiency, wavelet based methods are multiscale. This can partially enriches their representation ability and widens the effective processing area.

The main steps of wavelet denoising (also known as wavelet shrinkage) [2] are transforming the noisy image, denoising detail subbands through a thresholding operator, and computing the inverse wavelet transform. Despite the advantages of these methods, annoying visual artifacts are inevitable, which can be attributable to 1) rough frequency cut-offs due to thresholding operations, and 2) restricted representation ability. Statistical modeling is the main approach to improve the quality of thresholding [3–5]. It has been shown that considering the intrascale and interscale correlations of wavelet coefficients is very effective (e.g., BLS-GSM [6]). There are also attempts to reduce artifacts through variational methods [7,8], introducing redundancy in the denoising process [9], and using redundant wavelet transforms [10–13].

Despite tremendous efforts made over the years to improve wavelet denoising, their representation ability is intrinsically restricted since these transforms are not data adaptive. In contrast, synthesis sparse models [14–16] provide an adaptive framework to exploit the notion of sparsity. To enjoy both simplicity of sparse coding and adaptivity to data, the authors in [17–19] present the sparsifying transform learning model. They have shown that their model has comparable or even better performance compared to the well-known K-SVD synthesis dictionary learning [15,16]. However, both mentioned data-driven sparse models (dictionary learning and sparsifying transform learning) are inherently single-scale.

Image denoising methods often involve patch-based (or local) operations. When noise is weak, local modeling can achieve plausible results. However, as noise level increases, local image structures are substantially distorted by noise, and thus denoising through local operations becomes difficult. In this case, enlarging the effective modeling and denoising regions through multiscale processing is effective [20,21,30–34,22–29]. Also, it is shown that focusing on removing noise from high-frequency contents in the most patch-based methods lead to considerable artifacts and low-frequency content loss [20–25]. Even non-local methods such as non-local means [35,36] and BM3D [37] could not sufficiently reduce these types of artifacts [22,28]. Nevertheless, promising results have been reported in several multiscale methods [22–28]. Some representative works include the multiscale meta-procedure proposed by [25], multiscale K-SVD (MS K-SVD) [27], Fused K-SVD [28], multiscale EPLL (MSEPLL) [22], conservative scale recomposition [23], MS DCT [24], and MSND [31]. Most of these methods adopt

the pyramid image representation as a way to construct their multiscale methods. In contrast, MS K-SVD and Fused K-SVD exploit the wavelet transform. Since various forms of wavelet transforms and filter banks were proposed over the years, these approaches have a potential to boost denoising methods for different types of images. However, the former is generally suffers from considerable artifacts, and the latter is computationally demanding.

Here, our goal is to analyze and extend the subband denoising approach which was initially proposed by MS K-SVD [27]. In our first proposed method, similar to Fused K-SVD [28], we combine the results of single and multiscale denoising methods using a fusion method based on the wavelet subbands mixing technique [38,39]. This method greatly suppresses undesirable artifacts, while unlike the joint sparsity model in Fused K-SVD [28], it is very fast with favorably comparable results. Nevertheless, the whole method is still costly since it needs to denoise the image itself and all of its subbands (the approximate and detail subbands). Then, we simplify the operations and develop a new method in which there is no need to explicitly denoise detail subbands. This latter method saves the computational cost of denoising detail subbands, and it shows a systematic way of exploiting the pyramid of low-pass subbands of discrete wavelet transform for image denoising. We analyze and examine our studied methods on multiple image datasets with different natures. The overall qualitative and quantitative comparisons reveal that our methods offer a good trade-off between performance and complexity.

The rest of this paper is organized as follows. In the following section, we briefly review the related works. Next, we describe the studied multiscale methods in Section 3. Then, the experimental results are presented in Section 4 and the paper is concluded in Section 05.

2 RELATED WORKS

In this section, we review the sparsifying transform learning denoising [17–19] framework which is used as our primary single-scale denoising method due to its speed and numerical advantages over K-SVD. However, in the rest of this paper, whenever K-SVD performs better, we also report our results based on it. For K-SVD, we refer readers to [16]. In addition, we review some previous works on multiscale data-driven sparsity based methods.

2.1 SPARSIFYING TRANSFORM LEARNING DENOISING (TLD)

Transform models [17–19] assumes that signals of interest can be approximately sparsifiable using a transform matrix. Given a square transform matrix W ($m = n$) and sparse code x , the least squares estimate of the underlying signal vector u is obtained using $\hat{u} = W^\dagger x$, where W^\dagger denotes pseudoinverse of W . Ideally, in the transform model, corruptions such as noise cannot be well approximated in the transform domain, thus finding the sparse code of a corrupted signal over a suitable transform helps to restore it. Therefore, in [17], an adaptive signal denoising method is proposed as follows:

$$\begin{aligned}
& \min_{W, X, \hat{U}} \|WY - X\|_F^2 + \lambda Q(W) + \tau \|Y - \hat{U}\|_F^2 \\
& \text{s.t. } \|X_i\|_0 < l_i \quad \forall i
\end{aligned} \tag{1}$$

where $Y \in \mathbb{R}^{n \times N}$ is a matrix whose columns represent N signals corrupted by additive white Gaussian noise, and $\hat{U} \in \mathbb{R}^{n \times N}$ is a matrix containing recovered signals, $Q(W) = -\log|\det W| + \mu \|W\|_F^2$ is a regularizer to prevent trivial solutions, and the parameter τ is chosen inversely proportional to noise level σ .

To use the above formula for image denoising, the observed image Y is first divided using $R_i y$ into small overlapping patches of size $\sqrt{n} \times \sqrt{n}$, with R_i being the patch extraction operator and y being the vector form of image. Then, the mean intensity of each patch is removed, and all extracted patches $Y_i = R_i y$ are arranged as columns of the matrix Y . Next, the problem (1) is solved using an alternating optimization algorithm which alternates between a transform learning step and a variable sparsity update step.

The transform learning step is composed of a sparse coding step and a transform update step. Both steps are exactly solved using closed-form solutions [19]. The sparse codes X_i are obtained by thresholding WY_i to the l_i largest magnitude coefficients, and the transform update can be solved through a closed-form [19] solution with global convergence guarantee.

In practice, it turns out that using fixed sparsity levels degrade denoising performance. Therefore, an efficient variable sparsity update step is also proposed in [17,18]. For fixed W and X_i ($i = 1, 2, \dots, N$), this step reduces to the least squares problem in the \hat{U}_i 's. Each \hat{U}_i is updated by adding one nonzero element at a time from WY_i to X_i , until the error measure $\|Y_i - \hat{U}_i\|$ falls below a given threshold $nc^2\sigma^2$; where c is a fixed constant which controls the sparsity of representations. Finally, when all the estimated patches \hat{U}_i are recovered, the denoised image \hat{U} can be obtained by adding back the mean intensities to the final estimates and averaging them at their respective locations in the image.

2.2 MULTISCALE DATA-DRIVEN SPARSE MODELS

There are promising efforts to integrate multiscale analysis with data-driven sparse models [26–28,40–45]. The idea of learning sparse multiscale image representations dates back to the works of [40,41]. They show how a wavelet basis can be adapted to the statistics of natural images, and achieve slightly better coding efficiency [40] and denoising [41]. But these methods are fairly elaborate and computationally demanding since they rely on the sampling techniques to infer sparse codes. The work by [26] extends K-SVD [15,16] to simultaneously use different sizes of atoms, each size corresponding to a different scale. Their method achieves very promising results, though it is computationally expensive.

In a different approach, data-driven sparse models are directly applied in the multi-resolution analysis domain [26–28,42–45]. In this way, the denoising method acts as a complex wavelet shrinkage operator and the frequency selectivity of wavelet

subbands acts as a divide and conquer strategy which could result in sparser representations. In [42], a method based on filtering principal component coefficients of wavelet packet subbands is presented. The work in [27] have successfully shown that the K-SVD denoising method [16] can be directly used to filter wavelet subbands. Their experiments show that MS K-SVD partially outperforms single-scale KSVD [16] due to better recovery of textures, edges, and main image structures. However, MS K-SVD's results suffer from artifacts [28,44,45]. The same approach is used in [43–45] by considering other techniques such as structural clustering, nonlocal self-similarity, and Bayesian learning of a dictionary in the domain of the Laplacian pyramid [46].

Instead of trying to enrich the subband denoising approach with different techniques, Fused K-SVD [28] uses a joint sparse representation based method to fuse the results of the single [16] and multiscale K-SVD [27] methods. The assumption is that the underlying structure between these two results are the same. Therefore, a joint sparse representation technique [47] can be used to recover the underlying image without artifacts. Although the artifacts are suppressed greatly, the computational cost increases significantly since the joint sparse representations are obtained using concatenated input vectors and dictionaries. We will show that this step can be efficiently replaced by a method based on the subbands mixing technique. As we will demonstrate in our experiments, the proposed method has favorably comparable performance in comparison with Fused K-SVD, while its computation is greatly cheaper.

3 THE METHODS

3.1 MULTISCALE TLD (MTLD)

In this section, we develop a multiscale extension for TLD, which we name it multiscale TLD (MTLD). MTLD is similar to MS K-SVD [27] except that uses TLD for subband denoising instead of K-SVD. Therefore, it is faster, and it does not depend on the learnt dictionaries. We use MTLD as our main multiscale baseline for further developments.

To derive MTLD, we first begin by applying an analytical transform to data matrix Y in the formula of sparsifying transform learning (1). Let the transform matrix W in (1) be the product of two different square transforms $B\Phi$, then:

$$\begin{aligned} \min_{B, X, \hat{U}} & \|B\Phi Y - X\|_F^2 + \lambda Q(B) + \tau \|Y - \hat{U}\|_F^2 \\ \text{s.t. } & \|X_i\|_0 < l_i \quad \forall i \end{aligned} \quad (2)$$

where, Φ is an efficient fixed analytical transform, and B is a transform that is to be learned from data.

To solve (2), the doubly sparse transform learning formulation [18] can be used in which the authors suggest to simultaneously encourage transform B and sparse code X matrices to be sparse. However, here we do not encourage B to be sparse because:

(1) if we encourage sparsity of the transform matrix B , the efficient closed-form solution for the transform update step [19]

cannot be used, and (2) the doubly sparse formulation works well for transform matrices (such as DCT) that can be applied directly to data. In the case of wavelets, transform matrices are relatively large, and therefore it is not straightforward to use the doubly sparse formulation. Instead, a more intuitive and simpler approach can be taken by learning a separate transform B_s for each wavelet subband [27]:

$$\begin{aligned} \min_{B_s, X_s, \hat{U}_s} & \|B_s(\Phi Y)_s - X_s\|_F^2 + \lambda Q(B_s) + \tau \|(\Phi Y)_s - \hat{U}_s\|_F^2 \\ \text{s.t. } & \|X_i\|_0 < l_i \quad \forall i, \forall s \end{aligned} \quad (3)$$

where subscript s indicates different wavelet subbands, and $(\Phi Y)_s$ denotes a matrix containing signal vectors of the s -th wavelet subband. The above formula is similar to (1) except that it learns multiple separate transforms in order to restore subbands. The above formula establishes MTLD a counterpart of MS K-SVD.

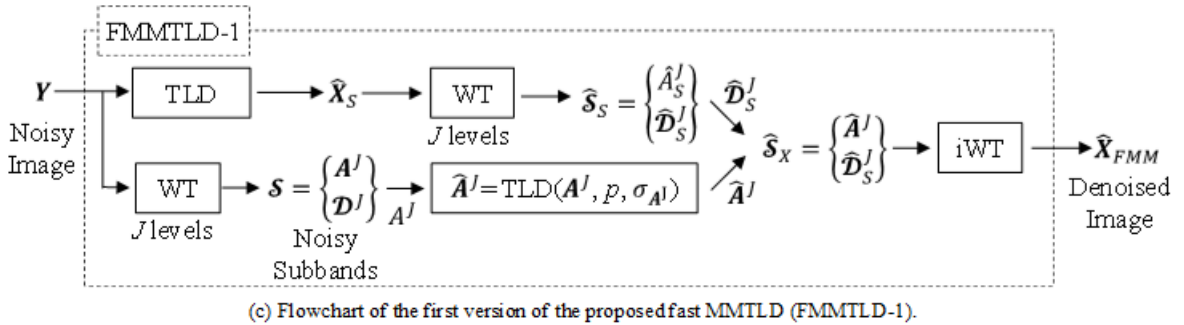
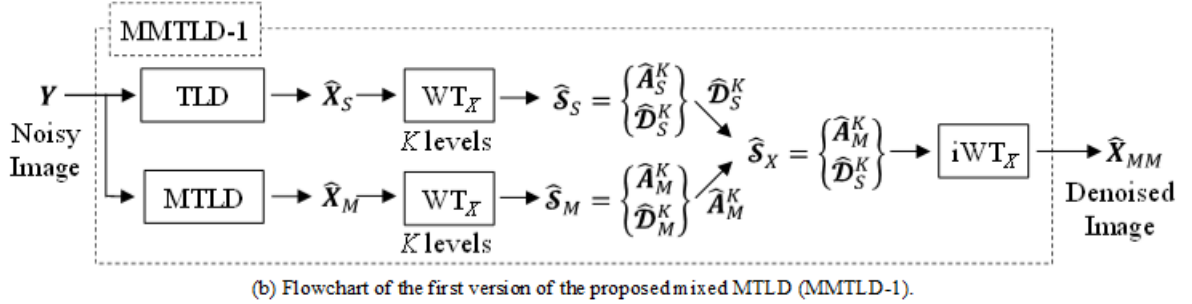
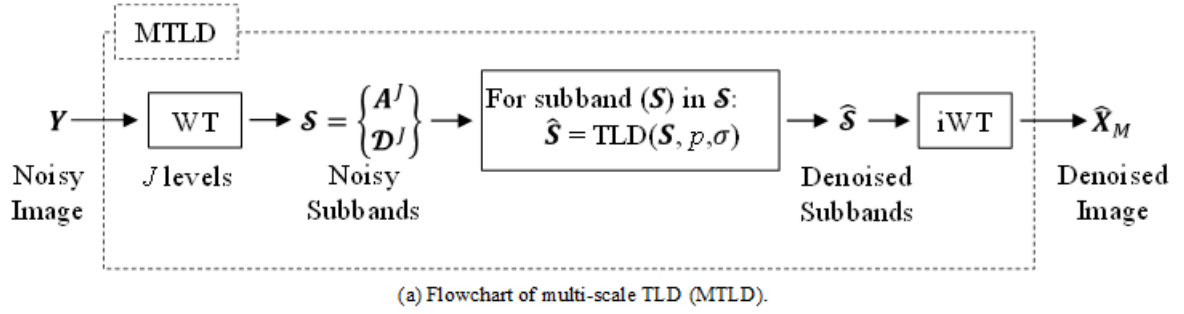


Fig. 1: Flowcharts of the multiscale sparsifying transform learning denoising (TLD) methods: (a) The multiscale TLD (MTLD) is developed exactly based on the idea of [27], and it is served as our multiscale baseline. In (b) and (c), the first versions of our proposed multiscale denoising methods (MMTLD-1 and FMMTLD-1) are shown. The (WT) and (WT_X) modules show a J -scale and a K -scale wavelet transforms, respectively. The corresponding inverse wavelet transforms are shown with (iWT) and (iWT_X).

3.1.1 MTLD STEPS AND ITS PARAMETERS

The outline of MTLD is shown in Fig. 1(a). It first applies a J -scale wavelet transform to the input image \mathbf{Y} and decomposes it into a set of subbands $\mathcal{S} = \{\mathbf{A}^J, \mathcal{D}^J\}$ which includes the approximate subband at scale J (\mathbf{A}^J) and a set (\mathcal{D}^J) containing the detail subbands, respectively. Next, each subband is denoised via TLD. Then, the denoised image ($\hat{\mathbf{X}}_M$) is reconstructed.

We list the MTLD steps more precisely in Algorithm 1. For implementing this method in practice, it is required to determine the type of the J -scale wavelet transform (line number #1) and its filter bank. These are hyper-parameters. While various wavelet transforms can be used to realize MTLD, here, the (WT) module (in Fig. 1 and Algorithm 1) is substituted with a J -scale discrete wavelet transform (DWT) [2] with the discrete Meyer analysis and synthesis filters (filter banks are denoted by afb and sfb in Algorithm 1).

MTLD calls TLD (in line number #4) to denoise subbands. TLD takes three inputs: noisy image (\mathbf{Y}), patch size (p), and standard deviation of noise (σ). Patch size is usually set to 11 x 11 pixels. The noise level (σ) is commonly assumed to be known or can be estimated by a noise estimation method [48,49]. However, MLTD needs noise levels of subbands (σ_S). Unlike the input image's noise level (σ), noise levels of subbands (σ_S) are not usually assumed to be known beforehand. Similar to MS K-SVD, we experimentally found that we can set $\sigma_S = \sigma$. This approach may not be optimal, but it suffices for the purpose of this study.

Algorithm 1 MTLD

Input:

Noisy image (\mathbf{Y}), Noise levels of subbands (σ_S), Patch size (p),
Number of scales (J)

Hyper-parameters:

Type of wavelet transform (WT) and its filter bank (the analysis
and synthesis filters are denoted by af , and sf , respectively).

Output:

Denoised Image ($\hat{\mathbf{X}}_M$)

```

1:  $\mathcal{S} = \text{WT}(\mathbf{Y}, J, af)$  //  $\mathcal{S}$  includes  $\{\mathbf{A}^J, \mathcal{D}^J\}$ .
2:  $\hat{\mathcal{S}} = \{\}$ 
3: For each subband ( $s$ ) in  $\mathcal{S}$ :
4:    $\hat{s} = \text{TLD}(s, \sigma_S, p)$ 
5:    $\hat{\mathcal{S}} = \hat{\mathcal{S}} \cup \hat{s}$ 
6:  $\hat{\mathbf{X}}_M = \text{iWT}(\hat{\mathcal{S}}, J, sf)$ 

```

3.1.2 MOTIVATIONAL EXAMPLE: MTLD VERSUS TLD

We show the outputs of TLD and MTLD for denoising a test image in Fig. 2 (b). In this example, MTLD is implemented with a 1-scale ($J=1$) DWT, and the results are shown in Fig. 2 (c) and (d). These results confirm that although the main image structures (or low-frequency information) are better recovered through MTLD, the artifacts in MTLD's output negatively affect the result. The quality of denoised images are quantized using the Peak Signal-to-Noise-Ratio (PSNR) and structural similarity index (SSIM) [50].

A number of reasons can be thought of for explaining why MTLD generally leads to inferior results than TLD: First, denoising a subband is not an easy task due to its low signal to noise ratio [22]. This is why a lot of efforts have been made over the years to introduce more effective wavelet shrinkage methods. Second, to denoise subbands using TLD, careful parameter adjustment for each subband might be required, which is a quite cumbersome procedure. These reasons may negatively contribute to the overall quality of MTLD.

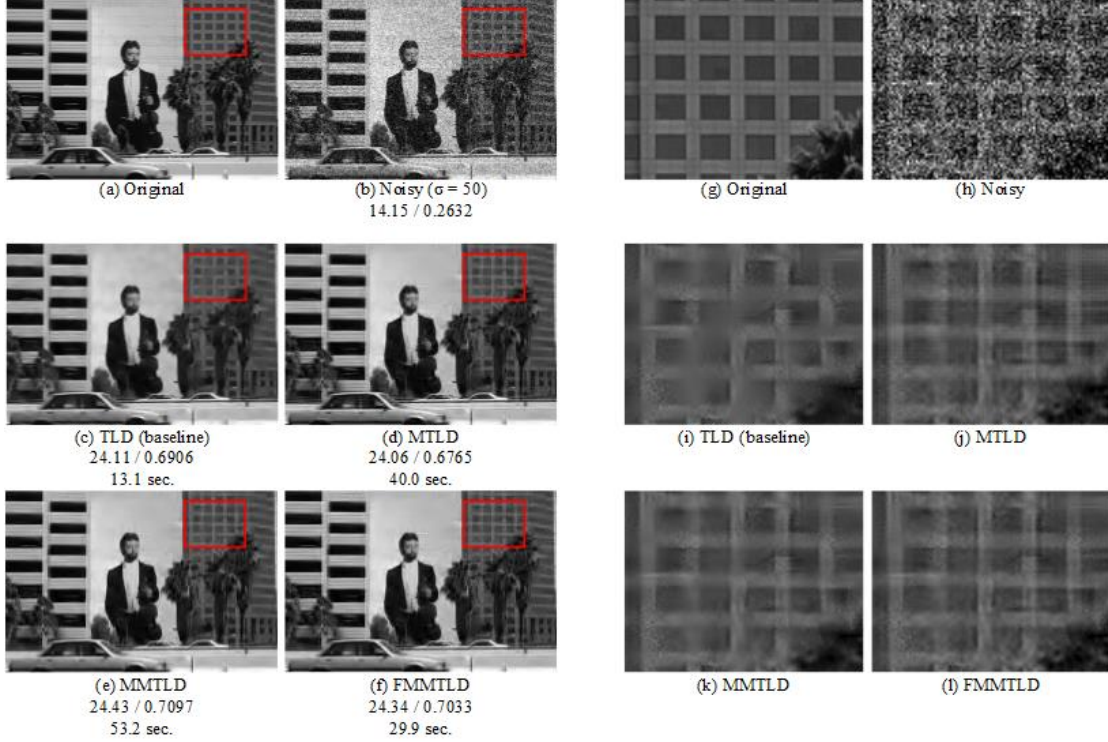


Fig. 2: Visual comparison of the denoising results by the studied methods. The original image is ‘test011’ from the BSD68 dataset. For each method, its PSNR, SSIM, and runtime are reported below it¹.

The above example shows that while the result of MTLD suffers from high frequency artifacts, the result of TLD do not suffer from such artifacts. TLD effectively removes high frequency noise, but it also removes the prominent image structures and degrades the low frequency contents.

In order to restore the damaged structures in Fig. 2 (c), a reader may suggest to carefully control the amount of denoising in TLD. This can be done by changing the c constant in TLD (Section 2.1). This constant controls the sparsity level, and it has a direct impact on the amount of denoising. To visually inspect the effects of different values of this hyper-parameter, we change it with steps of 0.05 in Fig. 3. Comparing Fig. 3 (b) and (c), it can be seen that although the default value of c is reasonable for this specific image, when we set c to 0.99 (Fig. 3 (b)), PSNR maximizes, and the damaged structures are better recovered.

¹ The runtimes reported throughout this paper were measured by running the experiments on a desktop PC. For more details, see Section 4.5.

However, note that this is achieved with the expense of decreasing SSIM and tolerating more artifacts. It turns out that even with this careful hyper-parameter adjustment, TLD cannot efficiently recover the damaged parts without sacrificing the quality.

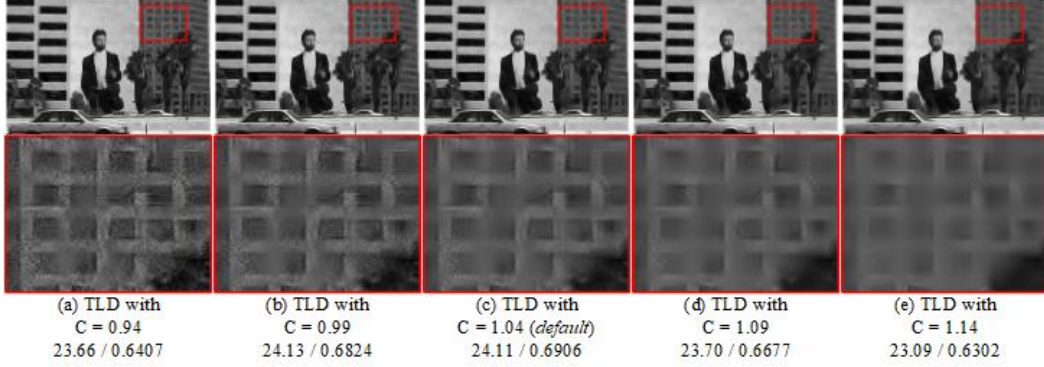


Fig. 3: Effects of using different sparsity levels (or error thresholds) on the output of TLD. The c constant (Section 2.1) modifies the sparsity level in TLD. By increasing this constant, the representations in TLD becomes sparser, and, therefore, noise suppression becomes stronger. For each method, its PSNR and SSIM are reported below it.

3.2 PROPOSED MIXED MTLD (MMTLD)

To overcome the aforementioned shortcomings and reconstruct a higher quality image, we here propose to exploit the wavelet subbands mixing technique [21], [22] as a cheap fusion technique in order to combine the merits of both TLD and MTLD: (i) The main image structure and low frequency contents of MTLD’s output, and (ii) The high frequency contents of TLD’s output. We call this method the Mixed MTLD (MMTLD) method, because it is based on mixing the subbands of TLD and MTLD methods.

The outline of our first version of MMTLD (denoted by MMTLD-1) is shown in Fig. 1 (b). The main steps are as follows. First, the outputs of TLD (\hat{X}_S) and MTLD (\hat{X}_M) are separately decomposed using a K -scale wavelet transform into their approximate and detail subbands. Then, the wavelet subbands mixing is applied to create a new set ($\hat{\mathcal{S}}_X$) which comprises of the approximate subband (\hat{A}_M^K) of MTLD and detail subbands (\hat{D}_S^K) of TLD. Finally, the inverse wavelet transform is computed on ($\hat{\mathcal{S}}_X$) to reconstruct the final denoised image (\hat{X}_{MM}).

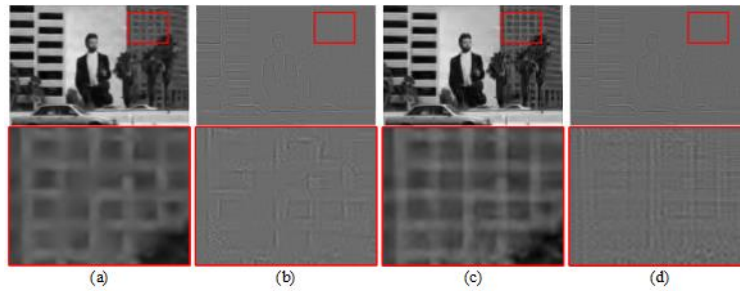


Fig. 4: Illustration of the subbands obtained by applying 1-scale ($K=1$) IUWT decompositions on TLD and MTLD outputs’. In the first two images, the TLD subbands are shown: (a) the approximate subband (\hat{A}_S^K), and (b) the detail subband (\hat{D}_S^K). In the last two images, the subbands of MTLD’s output are shown: (c) the approximate subband (\hat{A}_M^K), and (d) the detail subband (\hat{D}_M^K). In the mixing stage of MMTLD (Fig. 1 (b)), the method only uses (b) and (c) to reconstruct the final denoised image shown in Fig. 2 (e).

To demonstrate how the mixing stage of MMTLD-1 works in practice, let's use a 1-scale ($K=1$) isotropic undecimated wavelet transform (IUWT) with Astro filter bank [12] for implementing it. In each level, IUWT decomposes the input into one approximate and one detail subbands. In Fig. 4, the first row shows the subbands of TLD's output ($\widehat{\mathcal{S}}_S$) and the second row shows the subbands of MTLD's output ($\widehat{\mathcal{S}}_M$). It is evident that the low frequency contents in the approximate subband of MTLD (Fig. 4 (c)) is much richer than the corresponding subband of TLD (Fig. 4 (a)). Conversely, the detail subband of MTLD (Fig. 4 (d)) is noisier than corresponding subband of TLD (Fig. 4 (b)). Therefore, by taking the strength of both methods, MMTLD-1 avoids the weakness of MTLD in filtering detail subbands and the aggressive low frequency filtering of TLD.

3.3 PROPOSED FAST MMTLD (FMMTLD)

In the outline of MMTLD-1 (Fig. 1(b)), there are two types of wavelet transforms. The first one is in the denoising stage of MTLD and the second one is in the mixing stage of MMTLD-1. The former is a J -scale wavelet transform denoted by (WT) in Fig. 1(a), and the latter is a K -scale wavelet transform denoted by (WT _{X}) in Fig. 1(b). These two transforms are completely independent of each other, and we are free to choose the appropriate wavelet transform for each stage. However, when these two transforms are selected to be the same, considerable amount of computations become redundant since the set of detail subbands ($\widehat{\mathcal{D}}_M^K$) of MTLD is discarded in the mixing stage of MMTLD-1. Therefore, it is unnecessary to denoise them. To prove this claim, consider the following implication:

$$\text{When } \text{WT} = \text{WT}_X, \text{ then } \widehat{\mathcal{S}} = \widehat{\mathcal{S}}_M \quad (5)$$

where $\text{WT} = \text{WT}_X$ shows these transforms are identical (the same wavelet transform, filter bank, and number of scales), and

$\widehat{\mathcal{S}} = \widehat{\mathcal{S}}_M$ means that these two sets are equal.

Algorithm 2 FMMTLD-1

Input:

Noisy image (\mathbf{Y}) and its noise level (σ), Patch size (p),
Number of scales (J), Noise level (σ_{A^I}) of the approximate
subband at scale J .

Hyper-parameters:

Type of wavelet transform (WT) and its filter bank (the
analysis and synthesis filters are denoted by af , and sf ,
respectively).

Output:

Denoised Image ($\widehat{\mathbf{X}}_{FMM}$)

- 1: $\widehat{\mathbf{X}}_S = \text{TLD}(\mathbf{Y}, \sigma, p)$
 - 2: $\widehat{\mathcal{S}}_S = \text{WT}(\widehat{\mathbf{X}}_S, J, af)$ // $\widehat{\mathcal{S}}_S$ includes $\{\widehat{\mathbf{A}}_S^I, \widehat{\mathcal{D}}_S^I\}$.
 - 3: $\widehat{\mathcal{D}}_S^I = \text{Get the detail subbands from } \widehat{\mathcal{S}}_S$
 - 4: $\mathcal{S} = \text{WT}(\mathbf{Y}, J, af)$ // \mathcal{S} includes $\{\mathbf{A}^I, \mathcal{D}^I\}$.
 - 5: $\mathbf{A}^I = \text{Get the approximate subband from } \mathcal{S}$
 - 6: $\widehat{\mathbf{A}}^I = \text{TLD}(\mathbf{A}^I, \sigma_{A^I}, p)$
 - 7: $\widehat{\mathcal{S}}_X = \{\widehat{\mathbf{A}}^I, \widehat{\mathcal{D}}_S^I\}$
 - 8: $\widehat{\mathbf{X}}_{FMM} = \text{iWT}(\widehat{\mathcal{S}}_X, sf)$
-

The above implication holds since when these two transforms are identical, the inverse wavelet transform (iWT) at the end of MTLD (Fig. 1(a)) and the wavelet transform (WT_X) in the beginning of MMTLD-1 (Fig. 1(b)) cancels out each other (and $\widehat{\mathcal{S}}$ in MTLD becomes equivalent to $\widehat{\mathcal{S}}_M$ in MMTLD-1). In addition, since in the mixing stage of MMTLD-1, only the approximate subband (\widehat{A}_M^K) of MTLD is required, there is no need to denoise detail subbands (\widehat{D}_M^K) in MTLD (Fig. 1(a)).

The aforementioned discussion leads us to develop a more computationally efficient method which we name the Fast MMTLD (FMMTLD). An outline of the first version of FMMTLD is shown in Fig. 1(c). It consists of two branches. The first branch aims at obtaining denoised detail subbands (\widehat{D}_S^J). This is done indirectly, where the input image (Y) is denoised using TLD and then a J -scale wavelet transform (WT) is applied to the output of TLD (\widehat{X}_S) in order to decompose it into a set of wavelet subbands ($\widehat{\mathcal{S}}_S$). From this set, the detail subbands (\widehat{D}_S^J) are kept and the approximate subband (\widehat{A}_S^J) is discarded. In the second branch, the input image (Y) is first decomposed into the noisy wavelet subbands (\mathcal{S}), and then only the approximate subband (A^J) is denoised. Then, the method forms a new set ($\widehat{\mathcal{S}}_X$) from the denoised subbands. Finally, the inverse wavelet transform is computed to reconstruct the denoised image (\widehat{X}_{FMM}).

We also list the FMMTLD-1 steps more precisely in Algorithm 2. Similar to MTLD (Algorithm 1), we substitute (WT) with a J -scale DWT. A representative output of FMMTLD-1 (with $J=1$) is shown in Fig. 2 (f). It shows that FMMTLD-1 performs better than both TLD and MTLD, but worse than MMTLD-1. Better performance of MMTLD-1 can be attributable to the utilization of IUWT in its mixing stage. IUWT preserves translation-invariance property [12], and therefore it has less artifacts than DWT.

3.4 INCREASING THE NUMBER OF SCALES

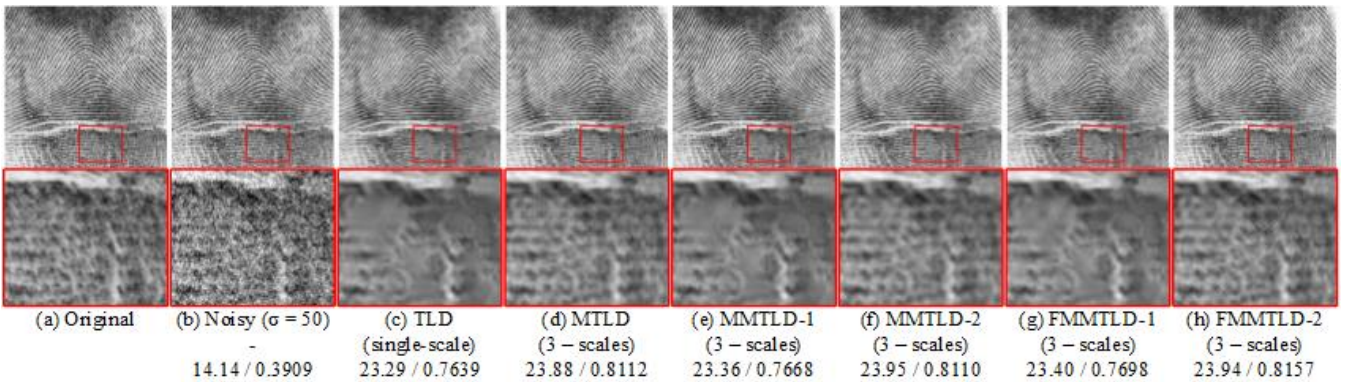


Fig. 5: Increasing the number of scales significantly reduces the effectiveness of multiscale processing in MMTLD-1 and FMMTLD-1. In this figure, we use wavelet transforms with 3 scales ($J=K=3$) to implement all methods, except TLD which is a single-scale method. The *fingerprint* image (a) is corrupted in (b) by adding a white Gaussian noise with $\sigma = 50$. For each method, its PSNR and SSIM are reported below it.

In our motivational example, all of the results (shown in Fig. 2) are obtained using 1-scale transforms. Specifically, we use a 1-scale DWT in the denoising stages of all methods, and we use a 1-scale IUWT and DWT in the mixing stages of MMTLD-

1 and FMMTLD-1, respectively. Naturally, we expect that by increasing the number of scales, more details can be recovered. In practice, the opposite happens, and the effect of multiscale processing is reduced by increasing the number of scales. For example, consider the results of MMTLD-1 and FMMTLD-1 with 3 scales in Fig. 5 (e) and (g). Comparing these results with MTLD (Fig. 5 (e)) and TLD (Fig. 5 (c)) reveal that the quality of the results of MMTLD-1 and FMMTLD-1 tend to TLD.

The source of this deficiency in MMTLD-1 and FMMTLD-1 lies in the mixing stage of these methods. As the number of scales increases, the approximate subband includes contents extracted from a smaller range of low frequencies, and a wider range of high frequency contents are placed into detail subbands. Since detail subbands are extracted from the output of the single-scale method (TLD), the contribution of the single-scale method in the final output of these methods grows with more scales.

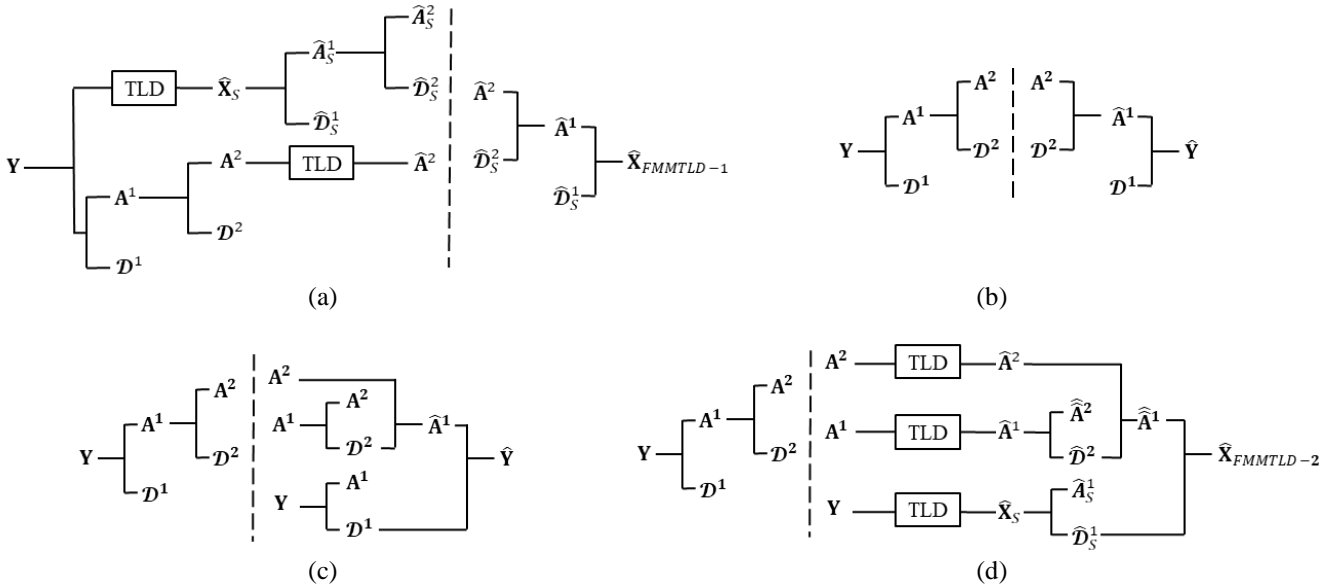


Fig. 6: Schematic diagrams of two-scale FMMTLD and Mallat's fast wavelet transform methods. (a) Diagram of FMMTLD-1 with a two-scale wavelet transform. (b) Diagram of Mallat's method for computing a two-scale discrete wavelet transform, and its inverse. (c) The inverse step of a wavelet transform is reformulated perform the reconstruction when the approximate subbands across different scales are taken as the input. (d) Diagram of implementing FMMTLD-2 with a two-scale wavelet transform. A hat (^) is used above the notation of each image/subband to denote that it is the output of either a denoising or an inverse wavelet transform step.

To fix FMMTLD-1, the detail subbands should be processed separately similar to MTLD. Consider a wavelet transform with two scales ($J = 2$). Then, the subbands are $\{A^2, D^2, D^1\}$. Now, let's compare the mixing stage of FMMTLD-1 and the reconstruction stage of the widely used Mallat's fast wavelet transform method [51]. We draw the schematic diagrams of a two-scale FMMTLD-1 and discrete wavelet transform in Fig. 6 (a) and (b), respectively. The vertical dashed line in Fig. 6 (a) separates the denoising (left) and mixing (right) stages of FMMTLD-1. Similarly, the vertical dashed line in Fig. 6 (b) separates the decomposition and reconstruction stages of the discrete wavelet transform. By comparing the right parts of these two

figures, it is evident that the mixing stage of FMMTLD-1 is nothing but an inverse wavelet transform on a set of selected denoised subbands ($\{\hat{\mathbf{A}}^2, \hat{\mathbf{D}}_S^1, \hat{\mathbf{D}}_S^2\}$).

Instead of using the last approximate subband (\mathbf{A}) and detail subbands ($\{\mathbf{D}_S^1, \mathbf{D}_S^2\}$), let's assume that we store the input image (\mathbf{Y}) as the zero-th approximate subband and all of its approximate subbands ($\{\mathbf{A}^1, \mathbf{A}^2\}$) across different scales. In this way, no information is lost. Then, to perform the inverse wavelet transform, we should reformulate the inverse transform as shown by the schematic diagram in Fig. 6 (c). In this diagram, the detail subband at each scale is extracted by applying a 1-scale wavelet decomposition on the approximate subband at the upper level (the finer scale). Clearly, this formulation is general, and can be used for arbitrary number of scales.

The formulation in Fig. 6 (c) allows us to denoise each detail subband indirectly, and simultaneously perform the subbands mixing. By inserting a denoising method for denoising each approximate subband, the diagram of the resultant method is shown in Fig. 6 (d). We call it FMMTLD-2. It is easy to see that when the number of scales is set to 1 ($J=1$), FMMTLD-2 is exactly equivalent to FMMTLD-1. However, in contrast to FMMTLD-1, when the number of scales is more than one, the denoising and mixing stages are applied for all of the approximate subbands at different scales. In Fig. 5 (g) and (h), the outputs of FMMTLD-1 and 2 are visually compared.

Algorithm 3 FMMTLD-2

Input:

Noisy image (\mathbf{Y}) and its noise level (σ), Patch size (p), Number of scales (J), Noise level (σ_{A^J}) of the approximate subband at scale J .

Hyper-parameters:

Type of wavelet transform (WT) and its filter bank (the analysis and synthesis filters are denoted by af , and sf , respectively).

Output:

Denoised Image ($\hat{\mathbf{X}}_{FMM}$)

```

1: AP[0] = {Y}                                // AP is an array
2: For s = 1 to J
3:   S = WT(AP[s - 1], 1, afb)                // 1-scale WT
4:   A = Get the approximate subband from S
5:   AP[s] = {A}

7: For s = J to 1
8:   AP[s - 1] = TLD(AP[s - 1],  $\sigma_{s-1}$ , p) // fine scale
9:   AP[s] = TLD(AP[s],  $\sigma_s$ , p)           // coarse scale

10:  Sf = WT(AP[s - 1], 1, afb)
11:  Df = Get the detail subbands from Sf
12:  Sc = WT(AP[s], 1, afb)
13:  Ac = Get the approximate subband from Sc
14:  Sx = {Ac, Df}
15:  AP[s - 1] = iWT(Sx, sfb)

16: XFMM = AP[0]
```

FMMTLD-2 steps are listed in Algorithm 3. The mechanism of this method is as follows: Firstly, it applies a 1-scale wavelet transform for J times (line number 1 to 5), and the noisy image and its approximate subbands across scales are stored in an

array (denoted by AP in Algorithm 3). The noisy image with the finest resolution is stored in AP[0] and the last approximate subband with the coarsest resolution is stored in AP[J]. Secondly, the method starts with the last two approximate subbands (AP[s-1] and AP[s]) and denoises them (line number 7 to 9). Thirdly, the method performs the subbands mixing. It reconstructs the denoised approximate subband at the finer scale (AP[s-1]) by changing its approximate subband with AP[s]. Finally, these steps are repeated across all scales to reconstruct the final image.

The same method can be used to fix MMTLD-1 (Fig. 1 (b)). MMTLD-1 combines the outputs of single-scale (TLD) and multiscale (MTLD) methods. In Algorithm 4, we list the steps of MMTLD-2 which performs the subbands mixing over multiple scales. Note that when $K=1$, this method reduces to MMTLD-1 (Fig. 1 (b)). The outputs of MMTLD-1 and MMTLD-2 are compared in Fig. 5 (e) and (f).

Algorithm 4 MMTLD-2

Input:

Noisy image (Y) and its noise level (σ), Patch size (p), Number of scales (J) for MTLD, Noise levels of subbands (σ_s), Number of scales (K) for the mixing stage.

Hyper-parameters:

Hyper-parameters of MTLD (See Algorithm 1), Type of wavelet transform (WT_X) and its filter bank for the mixing stage.

Output:

Denoised Image (\hat{X}_{MM})

```

1:  $\hat{X}_S = \text{TLD}(Y, \sigma, p)$ 
2:  $\hat{X}_M = \text{MTLD}(Y, \sigma_s, p, J)$ 

3: temp =  $\hat{X}_S$ 
4: For k = K to 1
5:    $\hat{\mathcal{S}}_S = WT_X(\text{temp}, k, af)$ 
6:    $\hat{\mathcal{D}}_S^k = \text{Get the detail subbands from } \hat{\mathcal{S}}_S$ 
7:    $\hat{\mathcal{S}}_M = WT_X(\hat{X}_M, k, af)$ 
8:    $\hat{\mathcal{A}}_M^k = \text{Get the approximate subband from } \hat{\mathcal{S}}_M$ 
9:    $\hat{\mathcal{S}}_X = \{\hat{\mathcal{A}}_M^k, \hat{\mathcal{D}}_S^k\}$ 
10:  temp =  $iWT_X(\hat{\mathcal{S}}_X, k, sf)$ 

11:  $\hat{X}_{MM} = \text{temp}$ 

```

4 EXPERIMENTAL RESULTS

In this section, we present the qualitative and quantitative results of the methods introduced in the previous section. The compared methods, datasets, and parameters are thoroughly discussed in the following subsections. The source code to reproduce the experiments will be made publicly available on the website: <https://github.com/ashkan-abbasi66>.

4.1 COMPARED METHODS

Until here, we have discussed four methods: TLD (Section 2.1), MTLD (Algorithm 1), MMTLD (Algorithm 4), and FMMTLD (Algorithm 3). As we have mentioned earlier, the proposed mixing based methods (MMTLD and FMMTLD) are quite general and we can embed another method such as K-SVD in place of our default single-scale denoiser (TLD). Therefore,

in the following experiments, we also report the results of MM K-SVD and FMM K-SVD wherever K-SVD performs better than TLD. MM K-SVD and FMM K-SVD are obtained by simply replacing TLD and MTLTLD in Algorithm 3 and 4 with K-SVD* and MS K-SVD [27], respectively. A star (*) above K-SVD indicate that its parameters are set different from the parameters of the official version of K-SVD [16]. K-SVD* was engineered to be used in MS K-SVD [27] and Fused K-SVD [28].

In the Gaussian denoising experiments (Section 4.3), we mainly compare the efficiency of TLD, MTLTLD, MMTLD, FMMTLTLD, MM K-SVD, and FMM K-SVD with three sparsity based image denoising methods as follows: BLS-GSM [6], MS K-SVD [27], and Fused K-SVD [28]. BLS-GSM is a benchmark wavelet thresholding based method, and the last two methods are multiscale dictionary learning based methods.

In microscopy image denoising experiments (Section 4.4), we compare the results of our TLD based methods (TLD, MTLTLD, MMTLD, FMMTLTLD) with the results of PURE-LET [52], K-SVD*, MS K-SVD, and Fused K-SVD. PURE-LET is a benchmark wavelet thresholding method for denoising images corrupted inherently with Poisson-Gaussian noise.

4.2 THE DATASETS

We evaluate the proposed methods over multiple datasets with different natures. First, we employ a set of 12 classic test images [22] to evaluate the effectiveness of the methods in removing synthetic Gaussian noise. Then, we employ a more realistic experiment of removing real Poisson-Gaussian noise from florescence microscopy images.

The classic test images are *Barbara*, *Boat*, *Cameraman*, *Fingerprint*, *Hill*, *House*, *Lena*, *Couple*, *Montage*, *Pentagon*, *Peppers*, and *Man*. We corrupt these images by adding white Gaussian noise with three standard deviations (15, 25, and 50) from relatively weak to strong noise levels.

As an instance of real world image denoising problem, we use the *mixed test set* from the recently published Fluorescence Microscopy Denoising (FMD) dataset [53]. These images are captured with three commercial microscopy imaging modalities (confocal, two-photon, and wide-field) from three representative biological samples, and they are inherently corrupted by real Poisson-Gaussian noise. The images captured from fixed bovine pulmonary artery endothelial (BPAE) cells are multi-channel (color), and the other images are gray-scale. The whole set consists of five subsets with decreasing noise levels. The first subset contains real noisy (raw) images, and the others were obtained by averaging 2, 4, 8, and 16 noisy images, respectively. Each subset has 48 noisy images. Also, there is a subset comprising of ground-truth images which are beneficial for quantitative evaluation of the performance of denoising methods.

4.3 GAUSSIAN IMAGE DENOISING

4.3.1 RESULTS

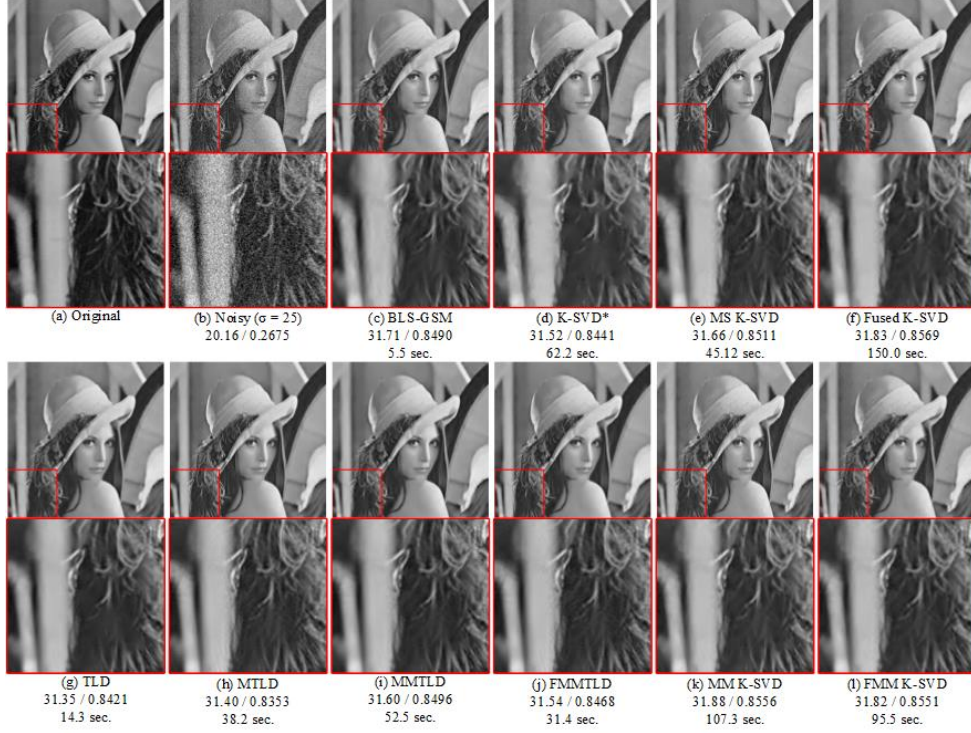


Fig. 7: Visual comparison of denoising results by the compared methods. The Lena image (a) is corrupted in (b) with additive white Gaussian noise with $\sigma = 25$. For each method, its PSNR, SSIM, and runtime are reported below it. Note to the competitive results of MM K-SVD and FMM K-SVD with Fused K-SVD, whereas our methods are more than 40 seconds faster.

Fig. 2 and 7 show some visual comparisons between the denoising outputs of the compared methods. The input image in Fig. 2 is corrupted with a relatively strong ($\sigma=50$) noise, and we have partially discussed about the performances of our TLD based methods in Section 3. The results of denoising through the compared methods are intentionally not reported. We will return to this example in the upcoming subsection (Fig. 9 in Section 4.3.2).

The input image in Fig. 7 (a) is corrupted with a medium noise level ($\sigma = 25$). In this figure, both MMTLD (Fig. 7 (i)) and FMMTLD (Fig. 7 (j)) improve the quality of denoised images significantly in comparison with their baselines (TLD and MTLD in Fig. 7 (g) and (h), respectively). Similar to Fig. 2, artifacts are responsible for the poor performance of MTLD and this weakness is mitigated in our proposed mixing based methods. However, both BLS-GSM (Fig. 7 (c)) and Fused K-SVD perform better than our best TLD based method (MMTLD). This is because of the poor performances of the baseline methods (TLD and MTLD). If we replace TLD and MTLD with K-SVD* and MS K-SVD, the resultant methods (MM K-SVD and FMM K-SVD) have competitive performances in comparison with BLS-GSM and Fused K-SVD. Note that the runtimes of MM K-SVD and FMM K-SVD are significantly lower than Fused K-SVD while their performances are very competitive.

Table 1

Mean of PSNR (dB), SSIM, and runtime of each method for Gaussian image denoising of two gray-scale datasets. The best PSNR and SSIM results are shown in **bold** and the second best results are underlined.

Dataset: 12 Classic Test Images				
Methods	15	25	50	Runtime
Noisy Images	24.61 / 0.5339	20.17 / 0.3535	14.16 / 0.1654	-
BLS-GSM	32.17 / 0.8750	29.71 / 0.8201	26.59 / 0.7243	6.0
K-SVD*	32.52 / 0.8809	29.97 / 0.8207	26.29 / 0.7114	80.4
MS K-SVD	32.21 / 0.8786	29.83 / 0.8261	26.76 / 0.7263	71.9
Fused K-SVD	<u>32.54 / 0.8846</u>	<u>30.11 / 0.8336</u>	<u>26.90 / 0.7426</u>	229.5
TLD	32.40 / 0.8798	29.75 / 0.8195	26.28 / 0.7097	16.9
MTLD	32.11 / 0.8739	29.61 / 0.8108	26.35 / 0.6847	48.4
MMTLD	32.47 / 0.8825	29.92 / 0.8264	26.61 / 0.7238	65.3
FMMTLD	32.38 / 0.8801	29.83 / 0.8222	26.54 / 0.7164	39.4
MM K-SVD	32.60 / 0.8851	30.23 / 0.8350	<u>26.92 / 0.7391</u>	152.4
FMM K-SVD	32.45 / 0.8819	30.08 / 0.8315	26.88 / 0.7366	120.0

The observations and explanations can be validated by the average quantitative results. We report the average PSNR, SSIM, and runtime for each denoising method in Table 1. It can be seen that, our MM K-SVD method generally outperforms the other methods. The second best method is Fused K-SVD which is very computationally expensive. TLD based methods are significantly faster than the K-SVD based methods, however, their results are inferior to them. The table also shows that MMTLD and MM K-SVD are slightly better than the corresponding fast methods. As we have mentioned earlier, this is due to using IUWT in the mixing stage.

The performance differences between our TLD and K-SVD based methods show that the performances of the mixing based methods are restricted by their baselines ((TLD and MTLD) or (K-SVD* and MS K-SVD)). This is clear because the high frequency contents are directly borrowed from the single-scale method (TLD or K-SVD*) and the low frequency contents are borrowed from the multi-scale method (MTLD or MS K-SVD). In the following subsection, we will discuss more about the effects of using various single-scale denoisers.

4.3.2 ROLE OF THE IMAGE DENOISER IN THE PERFORMANCE

To effectively compare the efficiency of the fusion/mixing based methods with each other, we plot the average PSNR gains obtained by these methods. In Fig. 8 (a), it is evident that, for all noise levels, MMTLD is better than its baselines (TLD and MTLD), and FMMTLD closely follows it. It can be seen that when noise is weak ($\sigma=15$), there is a 0.3 dB PSNR gap between MTLD and TLD. Therefore, it is hard for our mixing based methods to compensate this performance gap and produce better results. In fact, this shows that if MTLD works better, more performance gain can be obtained. In Fig. 8 (b), the average PSNR gains are shown for K-SVD based methods (Fused K-SVD, MM K-SVD, and FMM K-SVD). Note that how our proposed

mixing based methods closely follow the gains obtained by Fused K-SVD while our methods are much faster than it (Table 1).

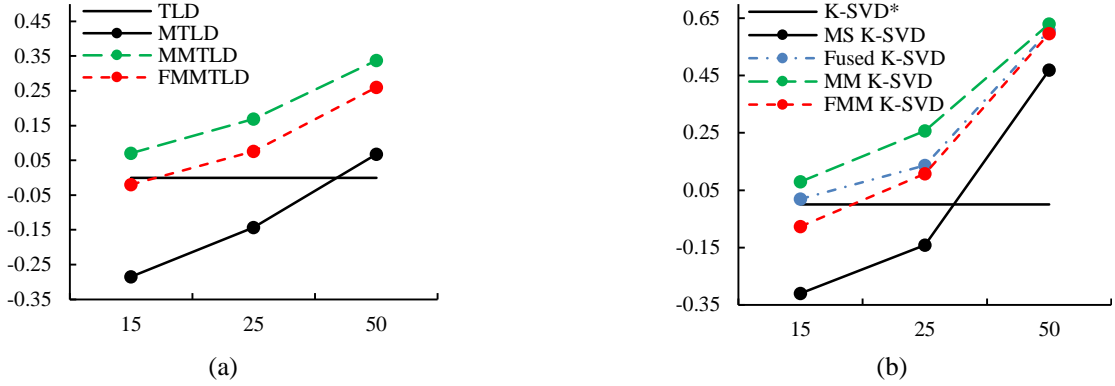


Fig. 8: The averaged PSNR gains obtained by the multiscale methods over their corresponding baselines. The horizontal axis shows different noise levels, and the vertical axis shows the average PSNR gains. The black horizontal line indicates the single-scale baseline method, and the black line with bullets indicates the gain that is obtained by the multiscale baseline method. In (a), the baselines are TLD and MTLTLD, and in (b), the baselines are K-SVD* and MS K-SVD. The colored dashed lines represent the gains of the fusion based methods.

Let's return to our motivational example (in Fig. 2). In Fig. 9 (a) to (f), we show visual comparisons of denoising the test image in Fig. 2 (b) through BLS-GSM, and the family of K-SVD based methods (K-SVD*, MS K-SVD, Fused K-SVD, MM K-SVD, and FMM K-SVD). It can be seen that our multiscale mixing based methods are better than MS K-SVD and Fused K-SVD.

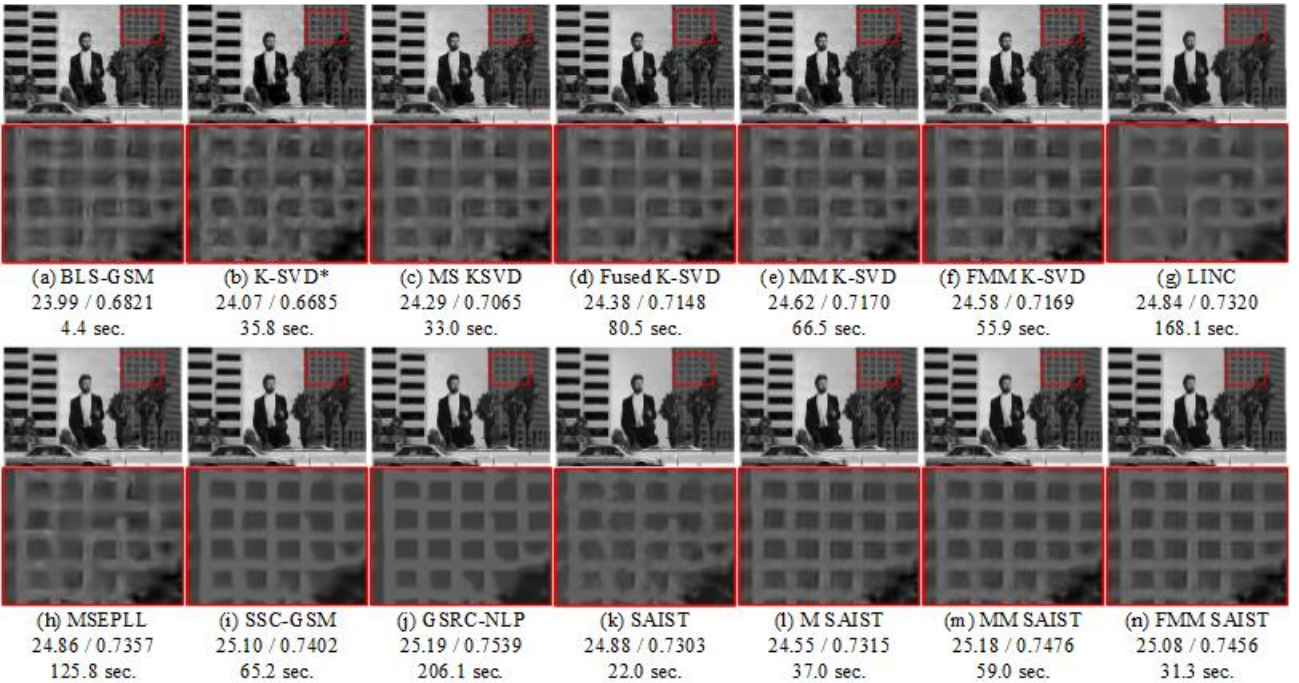


Fig. 9: Visual comparison of denoising results by the compared methods. The original image (a) is 'kodim15' from the Kodak dataset. The input image (b) is corrupted with additive white Gaussian noise with $\sigma = 15$. For each method, its PSNR, SSIM, and runtime are reported below it.

Until here, none of the mentioned methods exploits the self-similarity of images [36,54] which is a very powerful image prior formed by finding similar patches to a given patch. Therefore, our results are not competitive to the state-of-the-art denoising methods. Here, as an experiment to show the potential of our proposed mixing based methods in improving the results of single-scale denoisers, we use spatially adaptive iterative singular-value thresholding (SAIST) as our single-scale baseline. This method exploits simultaneous sparse coding of non-local similar patches through a low-rank modeling approach. We first use SAIST as our single-scale baseline method in place of TLD in Algorithm 1. We call the resultant method as M SAIST. Then, we use SAIST and M SAIST in place of TLD and MTLT in Algorithm 3 and Algorithm 4. The resultant methods are called FMM SAIST and MM SAIST. The outputs of denoising the test image in Fig. 2 through SAIST and its multiscale extensions are reported in Fig. 9 (f) to (i).

In Fig. 9, we can see that exploiting nonlocal similarities in companion with the multiscale information greatly improves the denoising result. The results of denoising the test image using some benchmark methods are also represented in Fig. 9 (g) to (j). Specifically, we report the results in the following order: Fig. 9 (g) shows the output of LINC [55] which is a Gaussian mixture model based method, Fig. 9 (h) shows the output of MSEPLL [22] which is the multiscale extension of the well-known expected log-likelihood (EPLL) method [56], Fig. 9 (i) shows the output of simultaneous sparse coding with Gaussian scale mixture method (SSC-GSM) [57], and Fig. 9 (j) shows the output of a recently proposed method named group sparsity residual constraint with nonlocal priors (GSRC-NLP). Note that how MM SAIST and FMM SAIST can compete with these methods, while our methods are faster.

The above example shows that although the proposed methods are introduced in the context of data-driven sparse methods such as dictionary or transform learning methods, they are quite general, and we can use an off-the-shelf denoiser as a single-scale baseline method. However, in practice, we found that it is not as straight forward as it seems to be. The main issue is how to effectively tune a single-scale baseline method to denoise subbands. In practice, it needs careful parameter or hyper-parameter adjustments to make a denoiser suitable for denoising the approximate or wavelet subbands. Although we haven't mentioned the average results of the multiscale extensions of SAIST here, we note that MM SAIST results are on average better than pure SAIST and MSEPLL, and inferior to SSC-GSM and GSRC-NLP. In the rest of this paper, unless explicitly mentioned, we use TLD and MTLT as our single-scale and multiscale methods due to their convenience and speed.

4.3.3 EFFECTS OF NUMBER OF DECOMPOSITION LEVELS

In this section, we experimentally study the effects of increasing the number of decomposition levels for denoising two classic images (*Lena*, and *Pentagon*) which have different spatial sizes (512x512, and 1024x1024, respectively). For simplicity,

we only corrupt these images with only one noise level ($\sigma = 50$), vary the number of decomposition levels from 1 to 5, and keep the other parameters fixed.

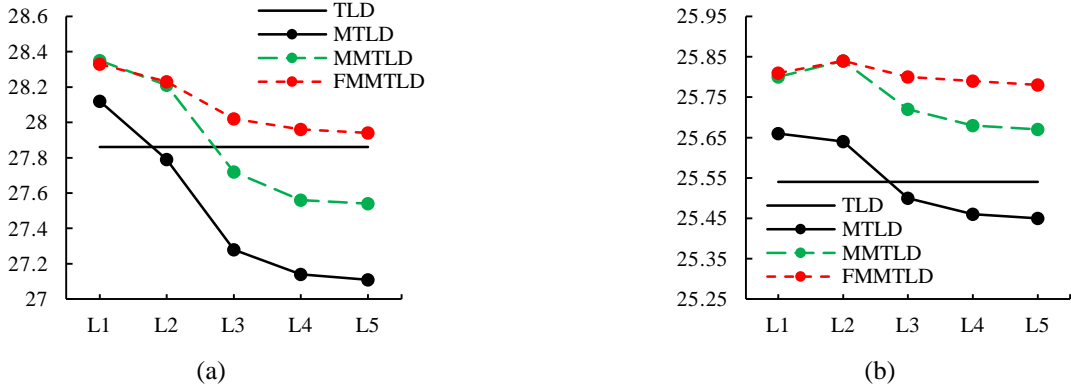


Fig. 10: Effects of the number of decomposition levels on the performances of the multiscale methods in comparison with the baseline. The horizontal axis indicates the number of scales used to perform the wavelet transform. The vertical axis shows PSNR results. In (a), the input image is *Lena* with spatial size of 512x512 pixels. The image is corrupted with Gaussian noise with $\sigma = 50$. In (b), the input image is *Pentagon* with spatial size of 1024x1024 pixels. The image is corrupted with Gaussian noise with $\sigma = 50$.

The plot of PSNR results obtained from denoising the mentioned test images are shown in **Error! Reference source not found.**. It can be seen that increasing the number of scales to more than one is just slightly beneficial for *Pentagon*. These plots show that MTLD’s quality drops quickly as the number of scales increases. In fact, MTLD’s deficiency negatively affect the quality of MMTLD.

It is worth mentioning that the criterion used in MS K-SVD [27] and Fused K-SVD [28] for selecting the number of scales is solely relied on the spatial size of the images. They experimentally observed that using their methods with more than one scale negatively affects the quality of denoising for images with width or height less than or equal to 550. Since we have used these methods for comparisons, except explicitly mentioned, we use this criterion for selecting the number of scales. Similar observations were also made in [22,26,45] where the authors have reported their final results based on using decompositions with 1 or 2 scales.

4.3.4 EFFECTS OF PATTERN SIZES: DENOISING A CHECKER BOARD IMAGE

It is reasonable that the image content is an important factor to determine whether multiscale denoising is beneficial or not. Here, we first synthetically create a checkerboard image (shown in Fig. 11 (a)) which includes five regions. Each region contains black and white square patterns with the same size. Next, the image is corrupted with additive white Gaussian noise with two levels. Then, we use our TLD based multiscale denoising methods to explicitly show that where multiscale patch-based denoising is beneficial. PSNR results of denoising the image corrupted with $\sigma=25$ and $\sigma=50$ are shown in Fig. 11 (b) and (c), respectively. Note that the actual patch size of our single-scale denoiser (TLD) is 11x11 pixels (Section 2.1). The plots in Fig. 11 (b) and (c) show that wherever the square patterns are smaller than or equal to the patch size (11x11), the

multiscale denoising is more beneficial. This is reasonable since when the patterns are big, learning a sparsifying transform to reconstruct big homogenous regions becomes an easy task. In this case, further processing by multiscale methods negatively affect the results. On the one hand, the effectiveness of MTLD and FMMTLD in recovering small details are comparable or even better than MMTLD. On the other hand, MMTLD's has a positive contribution for all patterns. This partially shows that why MMTLD has better performance in our previous experiments.

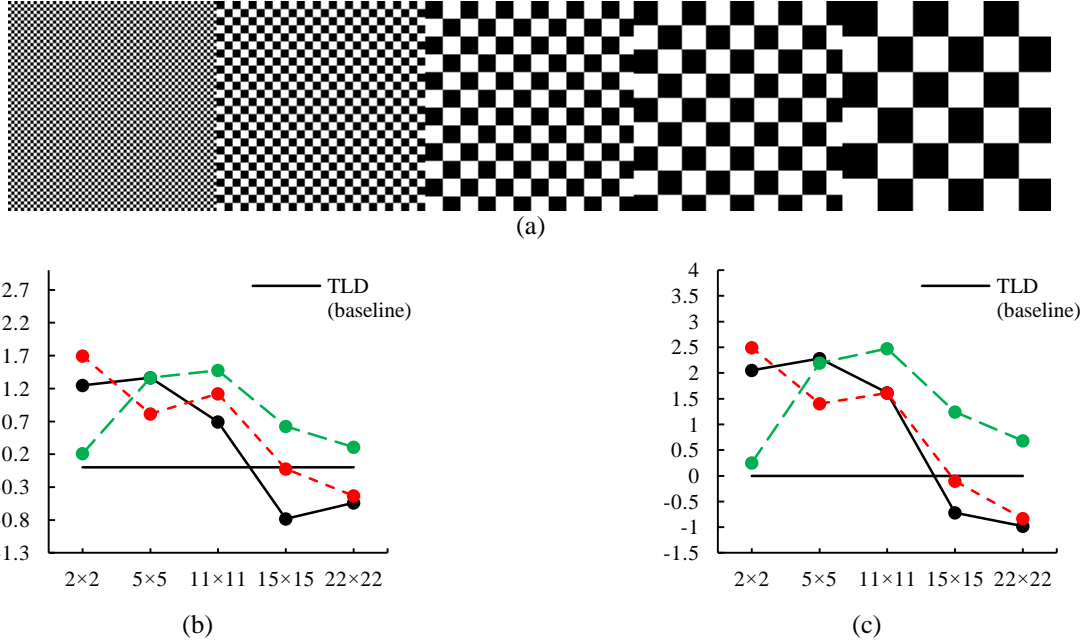


Fig. 11: Denoising a synthetic checkerboard image. In (a), the original image is shown. It consists of five different regions. Size of each region is 130×130 pixels, and each region is filled with black and white square patterns with the same size. The pattern sizes are as follows: 2×2 , 5×5 , 11×11 , 15×15 , and 22×22 pixels. The image (a) is corrupted with additive Gaussian noise with two standard deviations. Then, the PSNR gains over TLD (horizontal solid line) are reported in (b) and (c). In (b), PSNR gains are reported for denoising the image corrupted by $\sigma=25$, and, in (b), PSNR gains are reported for denoising the image corrupted with $\sigma=50$. Note that the PSNR gains are reported separately for the regions containing similar blocks with the sizes which are specified in the horizontal axis.

4.4 FLUORESCENCE MICROSCOPY IMAGE DENOISING

In this section, we generalize the applicability of our methods for denoising fluorescence microscopy images from the FMD dataset (described in Section 4.1) which are corrupted with real Poisson-Gaussian noise. Thus, the effectiveness and limitations of these methods are evaluated in a more real-world problem. In contrast to previous section (Gaussian image denoising), we will see that the FMMTLD's performance is closer to MMTLD. This is important since FMMTLD is significantly faster than MMTLD. This can be attributable to the efficiency of DWT's filter bank used for implementing FMMTLD in the microscopy images.

4.4.1 PARAMETERS OF THE COMPARED METHODS

Most of the parameters of the compared methods are set optimally or according to their papers. The parameters of TLD are set as described in Section 2.1 except for the constant c which determines the sparsity level in the variable sparsity update. Here, we set it to 0.98. Also, to implement the mixing stage in MMTLD, we experimentally found that the Astro filter bank (Section 3.2) is not suitable for analyzing fluorescence microscopy images and it leads to over smoothing. Thus, we implement IUWT using the Cohen-Daubechies-Fauveau 7/9 filter bank [13]. In this filter bank, the vector of 1-D low-pass filter coefficients is $[0, -0.04563588155, -0.02877176311, 0.295635881557, 0.557543526229, 0.295635881557, -0.02877176311, -0.04563588155, 0]$.

4.4.2 RESULTS

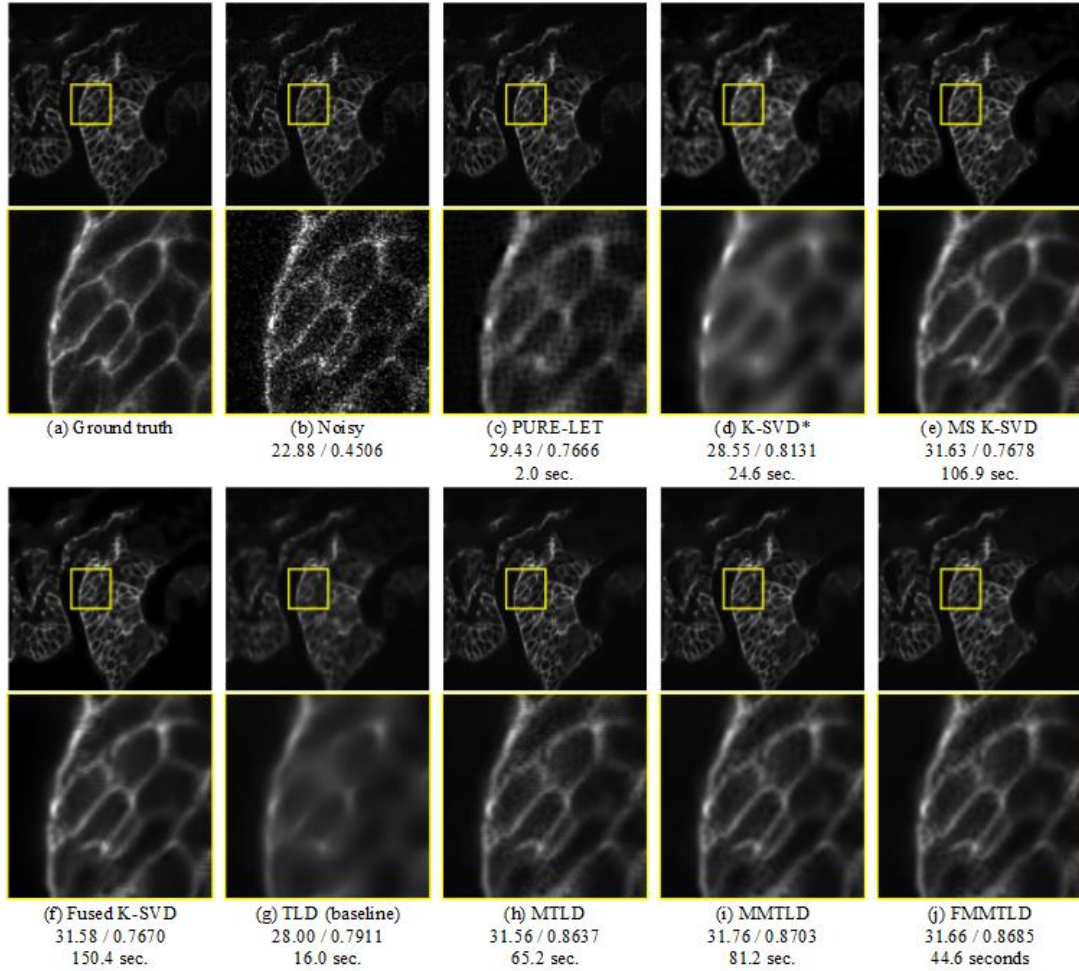


Fig. 12: Visual comparison of denoised images by the compared methods. The raw image (b) was captured from the Zebrafish embryo sample under confocal microscopy. For each image, the boxed region is magnified below it. For each method, its PSNR, SSIM, and runtime are reported below it.

We note that all of the compared methods, except PURE-LET, are basically Gaussian denoising methods. Therefore, we apply these methods after transforming the data using the generalized Anscombe transformation designed for Poisson-Gaussian noise [58]. Then, we use the exact unbiased inverse transformation [59] to transform back to the original domain.

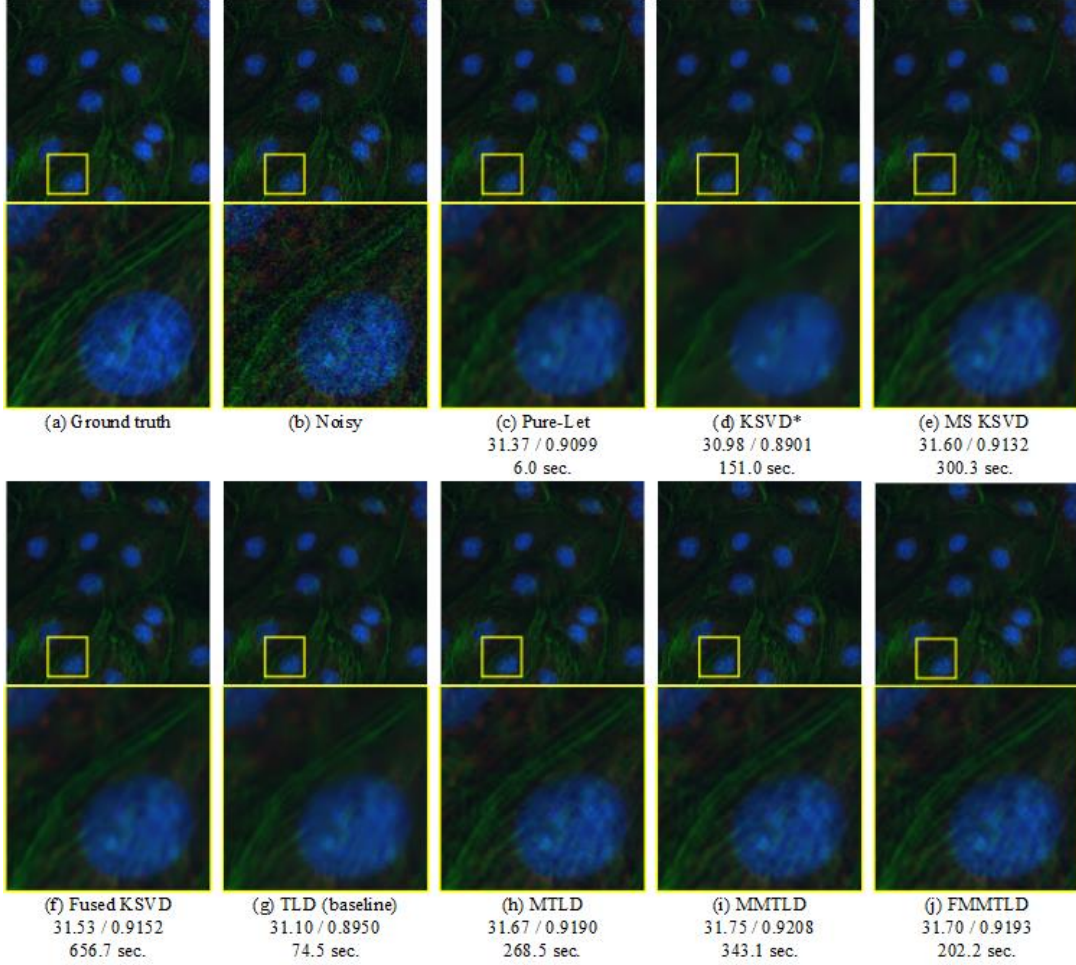


Fig. 13: Visual comparison of denoised images by the compared methods. The images are multi-channel. The raw image (b) was captured from the samples of BPAE cells under a two-photon microscopy. For each image, the boxed region is magnified below it. For each method, PSNR, SSIM, and its runtime are reported below it.

Visual results of denoising two fluorescence microscopy images are shown in Fig. 12 and 13. In Fig. 12, we show the results of denoising a representative single-channel fluorescence microscopy image (Fig. 12 (b)) which is a raw image of the Zebrafish embryo sample under a confocal microscopy. The noise in this image is relatively strong. Therefore, it is expected that the single-scale methods destroy image structures and over-smooth details. Fig. 12 (d) and (g) show that K-SVD* and TLD have poor performances. Edges and textures are better recovered using a multiscale approach like PURE-LET (Fig. 12 (c)). However, it also leads to visible artifacts which might be the result of using thresholding operator over a fixed wavelet bases. K-SVD's multiscale counterparts (MS K-SVD and Fused K-SVD) recover structures in Fig. 12 (e) and (f) with less artifacts, but the edges are somewhat blurry. In Fig. 12 (h), we can see that MTLD greatly enhances the results. Further improvements

achieve using both proposed multiscale mixing based methods (MTLD and FMMTLD). The visual and quantitative results show that the two proposed multiscale mixing based methods perform almost the same while there is a significant runtime advantage for FMMTLD in comparison with MTLD and MMTLD.

In Fig. 13, we show the results of denoising a representative multi-channel (color) fluorescence microscopy image. The original raw image (Fig. 13 (b)) is captured from the samples of BPAE cells under a two-photon microscopy. Each channel is independently denoised through the compared methods. Again, we can see that both single-scale methods (K-SVD and TLD) perform poorly in recovering details. PURE-LET does a better job at recovering details while its artifacts negatively affect the result. Again, it can be seen that the two proposed multiscale mixing based methods resolve have better denoising quality.

We note that, in case of Gaussian image denoising (Section 4.3), it is qualitatively and quantitatively confirmed that MTLD is inferior to TLD. The reason is the artifacts produced by MTLD cancels out the benefits of better structure recovery by it. However, for raw fluorescence microscopy images, Fig. 12 and 13 suggest that MTLD can produce better results than TLD. These results can be validated with computing the quantitative metrics over the whole dataset.

Table 2

Mean of the PSNR and SSIM results for denoising the mixed test set from FMD dataset through the compared methods. The best PSNR and SSIM results are shown in **bold** and the second best ones are underlined.

Methods	1	2	4	8	16	Runtime
Raw Images	27.22 / 0.5442	30.08 / 0.6800	32.86 / 0.7981	36.03 / 0.8892	39.70 / 0.9487	-
PURE-LET	31.95 / 0.7659	33.49 / 0.8267	35.29 / 0.8811	37.25 / 0.9210	39.59 / 0.9449	2.5
K-SVD*	31.89 / 0.7661	33.68 / 0.8311	35.81 / 0.8912	37.75 / 0.9301	40.26 / 0.9572	92.6
MS K-SVD	32.46 / 0.7791	33.81 / 0.8372	35.74 / 0.8939	37.62 / 0.9307	40.04 / 0.9566	147.7
Fused K-SVD	<u>32.54</u> / 0.7799	<u>33.88</u> / 0.8388	35.87 / 0.8949	37.75 / 0.9316	40.21 / 0.9574	333.3
TLD	31.95 / 0.7745	33.69 / 0.8340	35.86 / 0.8942	37.86 / 0.9324	40.43 / <u>0.9588</u>	45.2
MTLD	32.44 / 0.7854	33.89 / 0.8392	35.89 / 0.8950	37.91 / 0.9336	40.50 / 0.9603	144.5
MMTLD	32.55 / 0.7895	33.97 / 0.8419	35.98 / 0.8966	<u>37.97</u> / 0.9342	<u>40.55</u> / 0.9603	189.8
FMMTLD	32.53 / <u>0.7890</u>	33.97 / <u>0.8417</u>	35.98 / <u>0.8965</u>	37.98 / <u>0.9341</u>	40.56 / 0.9603	123.9

The average of PSNR and SSIM results are tabulated in Table 2. For each method, the average metric values are reported in five columns. These columns are corresponding to the five subsets of images in the FMD dataset (Section 4.1). From left to right, the noise level decreases and the first column represents the raw images with the highest noise level. Comparing the quantitative results of TLD and MTLD show that the multiscale processing is more effective in high-noise regimes. As the noise level decreases, the effectiveness of MTLD also decreases. Both of the proposed multiscale mixing based methods show reasonably well performance. Compared to TLD, the denoising quality of raw images via MMTLD and FMMTLD increases by more than 0.5 decibels (dB) in terms of PSNR. The results confirm that MMTLD and FMMTLD perform considerably better than MS K-SVD, Fused K-SVD, and PURE-LET. Contrary to the obtained results in Gaussian denoising, the results of MMTLD and FMMTLD are very close to each other while FMMTLD has much less computation. The slightly better

performance of MMTLD can be contributed to the usage of IUWT (which is a redundant wavelet transform) in its mixing stage.

4.5 RUNTIMES

Throughout this paper, we reported the runtimes of the compared methods in almost all experiments. All of our methods are implemented in MATLAB, and the experiments were conducted on a desktop PC with an Intel® i5-7400K CPU at 3.0 GHz and 16 GB of RAM.

We can summarize the key computations involved in our methods (MTLD, MMTLD, and FMMTLD) as follows: 1) forward wavelet transform, 2) inverse wavelet transform, and 3) denoising through TLD. From these operations, the most costly one is TLD. In MTLD (Algorithm 1), if we use a J -scale wavelet transform, the method runs TLD to denoise $3J + 1$ subbands (including the last approximate subband). To implement MTLD, we use DWT which is a non-redundant wavelet transform. Therefore, the wavelet subbands are smaller than the input image, and it is expected that the multiscale denoising via MTLD does not significantly increase the overall computations. However, in practice, the runtime of MTLD is considerably higher than TLD. For example, in Table 1, MTLD is implemented with a 1-scale DWT. Therefore, we might expect that each subband is denoised in one-fourth of the time of TLD but it takes more time. The reason lies in the different convergence behaviors. TLD’s runtime not only depends on the size of its input image but also on its content and noise level [19].

The runtime of MMTLD (Algorithm 4) is dominated by the runtimes of TLD and MTLD since MMTLD’s mixing stage is just involved with some cheap operations (forward wavelet transform and its inverse). In Table 1, it can be seen that by adding the runtimes of TLD and MTLD, the runtime of MMTLD can be well approximated. This shows that the whole mixing stage takes less than 0.1 second for the two datasets reported in this table.

Comparing the operations of FMMTLD (Algorithm 3) and MMTLD (Algorithm 4) shows that the main advantage of FMMTLD comes from the fact that it saves operations needed to denoise all detail subbands. Considering the fact that the bottleneck of MTLD and MMTLD are denoising wavelet subbands, it would be clear that FMMTLD suggests a significant reduction in the computational complexity. As mentioned earlier, this reduction in operations comes at the cost of restricting both denoising and mixing stages to use the same type of wavelet transform. Since FMMTLD works by denoising the pyramid of low-pass subbands (the input image and all of its low-pass subbands), it is theoretically $1 + 1/4 + 1/16 + \dots = 4/3$ more complex than TLD. However, due to the convergence issues of TLD that we have mentioned earlier, FMMTLD’s runtime is slightly bigger in practice (Table 1).

5 CONCLUSION

Sparsifying transform learning is a data-driven sparse model that can be efficiently used for adaptive image denoising [17–19]. However, similar to other data-driven sparse models [15,16], it is intrinsically single-scale. To exploit the multiscale nature of images in the transform learning denoising (TLD) and similar data-driven sparse models, this paper thoroughly investigates some methods. Specifically, three multiscale denoising methods are studied: MTLD, MMTLD, and FMMTLD. In multiscale TLD (MTLD), the method simply denoises all wavelet subbands through TLD. This approach, which is first introduced in [27] and further developed by [28], is simple and intuitive but it generally produces considerable artifacts that prevail over its effectiveness in recovering image details. Moreover, it is computationally demanding since it needs to denoise all subbands. To suppress these artifacts, we propose to use the wavelet subbands mixing technique [38,39] as a cheap fusion technique. Using this technique, the mixed MTLD (MMTLD) method takes the advantage of both TLD and MTLD methods and avoids their weaknesses. Comprehensive experiments over different datasets show that MMTLD can preserve image structures while greatly suppress artifacts. However, its computational cost is greater than MTLD which may hinder its application. We simplify this method and devise a method called fast MMTLD (FMMTLD). The main property of FMMTLD is that the method saves computations required to denoise detail subbands, leading to a simpler multiscale denoising method with close performance to MMTLD. Our experiments show that the proposed mixing based methods are capable of recovering the underlying image details and greatly suppress artifacts. In denoising real fluorescence microscopy images, FMMTLD shows very close performance to MMTLD with less computations. We also show that although the methods are introduced in the context sparsifying transform learning [17–19], our discussion can be generalized for other sparse models such as synthesis sparse models [17–19]. A future extension to this paper might be using some modern denoising approaches such as a deep learning based denoising method [60] in place of TLD in the frameworks of MMTLD and FMMTLD. We highlight the limitations of the proposed methods through extensive experiments. These limitations can be served as promising research directions. Moreover, we also note that the simplicity of FMMTLD suggests that it has a potential to be extended for three dimensional denoising.

ACKNOWLEDGMENT

This paper was supported by the National Natural Science Foundation of China under Grant No.61922029, and the National Natural Science Foundation under Grant No. 61771192. The authors also would like to thank Prof. Ravishankar and his colleagues for making their source code freely available.

REFERENCES

- [1] N. Ahmed, T. Natarajan, K. Rao, Discrete Cosine Transform, *IEEE Trans. Comput.* C-23 (1974) 90–93. doi:10.1109/T-C.1974.223784.
- [2] S. Mallat, *A wavelet tour of signal processing*, Elsevier, 1999.
- [3] D.L. Donoho, I.M. Johnstone, Adapting to unknown smoothness via wavelet shrinkage, *J. Am. Stat. Assoc.* 90 (1995) 1200–1224.
- [4] D.L. Donoho, J.M. Johnstone, Ideal spatial adaptation by wavelet shrinkage, *Biometrika.* 81 (1994) 425–455.
- [5] S.G. Chang, Bin Yu, M. Vetterli, Adaptive wavelet thresholding for image denoising and compression, *IEEE Trans. Image Process.* 9 (2000) 1532–1546. doi:10.1109/83.862633.
- [6] J. Portilla, V. Strela, M.J. Wainwright, E.P. Simoncelli, Image denoising using scale mixtures of Gaussians in the wavelet domain, *IEEE Trans. Image Process.* 12 (2003) 1338–1351. doi:10.1109/tip.2003.818640.
- [7] S. Durand, J. Froment, Artifact free signal denoising with wavelets, in: *IEEE Int. Conf. Acoust. Speech, Signal Process. Proc.*, 2001: pp. 3685–3688.
- [8] M. Li, S. Ghosal, Fast translation invariant multiscale image denoising, *IEEE Trans. Image Process.* 24 (2015) 4876–4887.
- [9] R.R. Coifman, D.L. Donoho, Translation-Invariant De-Noising, in: A. Antoniadis, G. Oppenheim (Eds.), *Wavelets Stat.*, Springer New York, New York, NY, 1995: pp. 125–150. doi:10.1007/978-1-4612-2544-7_9.
- [10] J.E. Fowler, The redundant discrete wavelet transform and additive noise, *IEEE Signal Process. Lett.* 12 (2005) 629–632. doi:10.1109/LSP.2005.853048.
- [11] I.W. Selesnick, R.G. Baraniuk, N.C. Kingsbury, The dual-tree complex wavelet transform, *IEEE Signal Process. Mag.* 22 (2005) 123–151. doi:10.1109/MSP.2005.1550194.
- [12] J.-L. Starck, J. Fadili, F. Murtagh, The Undecimated Wavelet Decomposition and its Reconstruction, *IEEE Trans. Image Process.* 16 (2007) 297–309. doi:10.1109/TIP.2006.887733.
- [13] J.-L. Starck, F. Murtagh, J. Fadili, *Sparse image and signal processing: Wavelets and related geometric multiscale analysis*, Cambridge university press, 2015.
- [14] B.A. Olshausen, D.J. Field, Emergence of simple-cell receptive field properties by learning a sparse code for natural images, *Nature.* 381 (1996) 607–609. doi:10.1038/381607a0.
- [15] M. Aharon, M. Elad, A. Bruckstein, K-SVD: An algorithm for designing overcomplete dictionaries for sparse representation, *IEEE Trans. Signal Process.* 54 (2006) 4311–4322. doi:10.1109/TSP.2006.881199.

- [16] M. Elad, M. Aharon, Image Denoising Via Sparse and Redundant Representations Over Learned Dictionaries, *IEEE Trans. Image Process.* 15 (2006) 3736–3745.
- [17] S. Ravishankar, Y. Bresler, Learning Sparsifying Transforms, *IEEE Trans. Signal Process.* 61 (2013) 1072–1086. doi:10.1109/TSP.2012.2226449.
- [18] S. Ravishankar, Y. Bresler, Learning Doubly Sparse Transforms for Images, *IEEE Trans. Image Process.* 22 (2013) 4598–4612. doi:10.1109/TIP.2013.2274384.
- [19] S. Ravishankar, Y. Bresler, Sparsifying Transform Learning With Efficient Optimal Updates and Convergence Guarantees, *IEEE Trans. Signal Process.* 63 (2015) 2389–2404. doi:10.1109/TSP.2015.2405503.
- [20] M. Lebrun, M. Colom, A. Buades, J.M. Morel, Secrets of image denoising cuisine, *Acta Numer.* 21 (2012) 475–576. doi:10.1017/S0962492912000062.
- [21] M. Lebrun, M. Colom, J. Morel, Multiscale Image Blind Denoising, *IEEE Trans. Image Process.* 24 (2015) 3149–3161. doi:10.1109/TIP.2015.2439041.
- [22] V. Pappyan, M. Elad, Multi-Scale Patch-Based Image Restoration, *IEEE Trans. Image Process.* 25 (2016) 249–261. doi:10.1109/TIP.2015.2499698.
- [23] G. Facciolo, N. Pierazzo, J.-M. Morel, Conservative scale recomposition for multiscale denoising (the devil is in the high frequency detail), *SIAM J. Imaging Sci.* 10 (2017) 1603–1626.
- [24] N. Pierazzo, J.-M. Morel, G. Facciolo, Multi-scale DCT denoising, *Image Process. Line.* 7 (2017) 288–308.
- [25] H.C. Burger, S. Harmeling, Improving denoising algorithms via a multi-scale meta-procedure, in: *Jt. Pattern Recognit. Symp.*, 2011: pp. 206–215.
- [26] J. Mairal, G. Sapiro, M. Elad, Learning Multiscale Sparse Representations for Image and Video Restoration, *Multiscale Model. Simul.* 7 (2008) 214–241. doi:10.1137/070697653.
- [27] B. Ophir, M. Lustig, M. Elad, Multi-Scale Dictionary Learning Using Wavelets, *IEEE J. Sel. Top. Signal Process.* 5 (2011) 1014–1024. doi:10.1109/JSTSP.2011.2155032.
- [28] J. Sulam, B. Ophir, M. Elad, Image denoising through multi-scale learnt dictionaries, in: *IEEE Int. Conf. Image Process.*, IEEE, 2014: pp. 808–812. doi:10.1109/ICIP.2014.7025162.
- [29] U. Rajashekar, E.P. Simoncelli, Multiscale Denoising of Photographic Images, in: A. Bovik (Ed.), *Essent. Guid. to Image Process.*, Elsevier, Boston, 2009: pp. 241–261. doi:10.1016/B978-0-12-374457-9.00011-1.
- [30] M. Zontak, I. Mosseri, M. Irani, Separating Signal from Noise Using Patch Recurrence across Scales, in: *Proc. IEEE Conf. Comput. Vis. Pattern Recognit.*, 2013.

- [31] W. Feng, P. Qiao, X. Xi, Y. Chen, Image Denoising via Multi-scale Nonlinear Diffusion Models, CoRR. abs/1609.0 (2016). <http://arxiv.org/abs/1609.06585>.
- [32] T. Remez, O. Litany, R. Giryes, A.M. Bronstein, Class-Aware Fully Convolutional Gaussian and Poisson Denoising, IEEE Trans. Image Process. 27 (2018) 5707–5722. doi:10.1109/TIP.2018.2859044.
- [33] S. Lefkimmatis, P. Maragos, G. Papandreou, Bayesian Inference on Multiscale Models for Poisson Intensity Estimation: Applications to Photon-Limited Image Denoising, IEEE Trans. Image Process. 18 (2009) 1724–1741. doi:10.1109/TIP.2009.2022008.
- [34] Xianming Liu, Deming Zhai, Debin Zhao, Guangtao Zhai, Wen Gao, Progressive Image Denoising Through Hybrid Graph Laplacian Regularization: A Unified Framework, IEEE Trans. Image Process. 23 (2014) 1491–1503. doi:10.1109/TIP.2014.2303638.
- [35] A. Buades, B. Coll, J.-M. Morel, Non-Local Means Denoising, Image Process. Line. 1 (2011) 490–530. doi:10.5201/ipol.2011.bcm_nlm.
- [36] A. Buades, B. Coll, J.M. Morel, A Review of Image Denoising Algorithms, with a New One, Multiscale Model. Simul. 4 (2005) 490–530. doi:10.1137/040616024.
- [37] K. Dabov, A. Foi, V. Katkovnik, K. Egiazarian, Image Denoising by Sparse 3-D Transform-Domain Collaborative Filtering, IEEE Trans. Image Process. 16 (2007) 2080–2095.
- [38] A. Lukin, A Multiresolution Approach for Improving Quality of Image Denoising Algorithms, in: IEEE Int. Conf. Acoust. Speed Signal Process. Proc., IEEE, 2006: pp. II-857-II-860. doi:10.1109/ICASSP.2006.1660478.
- [39] P. Coupé, P. Hellier, S. Prima, C. Kervrann, C. Barillot, 3D Wavelet Subbands Mixing for Image Denoising, Int. J. Biomed. Imaging. 2008 (2008) 1–11. doi:10.1155/2008/590183.
- [40] B.A. Olshausen, P. Sallee, M.S. Lewicki, Learning sparse image codes using a wavelet pyramid architecture, in: Adv. Neural Inf. Process. Syst., 2001: pp. 887–893.
- [41] P. Sallee, B.A. Olshausen, Learning sparse multiscale image representations, in: Adv. Neural Inf. Process. Syst., 2003: pp. 1351–1358.
- [42] S. Bacchelli, S. Papi, Image denoising using principal component analysis in the wavelet domain, J. Comput. Appl. Math. 189 (2006) 606–621. doi:10.1016/j.cam.2005.04.030.
- [43] L. Fang, S. Li, Q. Nie, J.A. Izatt, C.A. Toth, S. Farsiu, Sparsity based denoising of spectral domain optical coherence tomography images., Biomed. Opt. Express. 3 (2012) 927–42. doi:10.1364/BOE.3.000927.
- [44] R. Yan, L. Shao, Y. Liu, Nonlocal Hierarchical Dictionary Learning Using Wavelets for Image Denoising, IEEE Trans.

Image Process. 22 (2013) 4689–4698. doi:10.1109/TIP.2013.2277813.

- [45] J.M. Hughes, D.N. Rockmore, Y. Wang, Bayesian Learning of Sparse Multiscale Image Representations, IEEE Trans. Image Process. 22 (2013) 4972–4983. doi:10.1109/TIP.2013.2280188.
- [46] P. Burt, E. Adelson, The Laplacian Pyramid as a Compact Image Code, IEEE Trans. Commun. 31 (1983) 532–540. doi:10.1109/TCOM.1983.1095851.
- [47] N. Yu, T. Qiu, F. Ren, Denoising for Multiple Image Copies through Joint Sparse Representation, J. Math. Imaging Vis. 45 (2013) 46–54. doi:10.1007/s10851-012-0343-1.
- [48] A. Foi, Noise estimation and removal in MR imaging: The variance-stabilization approach, in: Proc. IEEE Int. Symp. Biomed. Imaging From Nano to Macro, 2011: pp. 1809–1814.
- [49] M. Rakhshanfar, M.A. Amer, Estimation of Gaussian, Poissonian-Gaussian, and Processed Visual Noise and its Level Function, IEEE Trans. Image Process. 25 (2016) 1–1. doi:10.1109/TIP.2016.2588320.
- [50] Z. Wang, A.C. Bovik, H.R. Sheikh, E.P. Simoncelli, Image Quality Assessment: From Error Visibility to Structural Similarity, IEEE Trans. Image Process. 13 (2004) 600–612. doi:10.1109/TIP.2003.819861.
- [51] S.G. Mallat, A theory for multiresolution signal decomposition: the wavelet representation, IEEE Trans. Pattern Anal. Mach. Intell. 11 (1989) 674–693. doi:10.1109/34.192463.
- [52] F. Luisier, T. Blu, M. Unser, Image Denoising in Mixed Poisson–Gaussian Noise, IEEE Trans. Image Process. 20 (2011) 696–708. doi:10.1109/TIP.2010.2073477.
- [53] Y. Zhang, Y. Zhu, E. Nichols, Q. Wang, S. Zhang, C. Smith, S. Howard, A Poisson-Gaussian Denoising Dataset With Real Fluorescence Microscopy Images, in: IEEE Conf. Comput. Vis. Pattern Recognit., IEEE, 2019: pp. 11702–11710. doi:10.1109/CVPR.2019.01198.
- [54] A. Buades, B. Coll, J.-M. Morel, A Non-Local Algorithm for Image Denoising, in: IEEE Conf. Comput. Vis. Pattern Recognit., IEEE, 2005: pp. 60–65. doi:10.1109/CVPR.2005.38.
- [55] M. Niknejad, H. Rabbani, M. Babaie-Zadeh, C. Jutten, Image Restoration Using Gaussian Mixture Models With Spatially Constrained Patch Clustering, in: IEEE Trans. Image Process., IEEE, 2015: pp. 3624–3636. doi:10.1109/TIP.2015.2447836.
- [56] D. Zoran, Y. Weiss, From learning models of natural image patches to whole image restoration, in: 2011 Int. Conf. Comput. Vis., IEEE, 2011: pp. 479–486. doi:10.1109/ICCV.2011.6126278.
- [57] W. Dong, G. Shi, Y. Ma, X. Li, Image Restoration via Simultaneous Sparse Coding: Where Structured Sparsity Meets Gaussian Scale Mixture, Int. J. Comput. Vis. 114 (2015) 217–232. doi:10.1007/s11263-015-0808-y.

- [58] F. Murtagh, J.-L. Starck, A. Bijaoui, Image restoration with noise suppression using a multiresolution support., *Astron. Astrophys. Suppl. Ser.* 112 (1995) 179.
- [59] M. Makitalo, A. Foi, Optimal Inversion of the Generalized Anscombe Transformation for Poisson-Gaussian Noise, *IEEE Trans. Image Process.* 22 (2013) 91–103. doi:10.1109/TIP.2012.2202675.
- [60] K. Zhang, W. Zuo, Y. Chen, D. Meng, L. Zhang, Beyond a Gaussian denoiser: Residual learning of deep CNN for image denoising, *IEEE Trans. Image Process.* 26 (2017) 3142–3155. doi:10.1109/TIP.2017.2662206.